Eur. Phys. J. D **36**, 179–185 (2005)
DOI: 10.1140/epjd/e2005-00264-8

THE EUROPEAN PHYSICAL JOURNAL D

Photodissociation of stored metal clusters

Fragment-abundance spectra after multisequential decay of Au_{30}^+

L. Schweikhard[1], K. Hansen[2], A. Herlert[1,a], M.D. Herráiz Lablanca[3], and M. Vogel[4]

[1] Institut für Physik, Ernst-Moritz-Arndt-Universität Greifswald, Domstr. 10a, 17487 Greifswald, Germany
[2] Department of Physics, Göteborg University, 41296 Gothenburg, Sweden
[3] Institut für Physik, Johannes Gutenberg-Universität, 55099 Mainz, Germany
[4] Imperial College London, Prince Consort Road, London SW7 2BW, UK

Received 3 June 2005 / Received in final form 18 August 2005
Published online 4 October 2005

Abstract. Ion trapping allows detailed studies of atomic clusters with various interactions and over a large range of timescales. An overview of methods at hand is given and a specific example is presented in detail where size-selected Au_{30}^+ clusters have been stored in a Penning trap and photofragmented by exposure to the third harmonic of a Nd:YAG laser. The resulting mass spectra were sampled after reaction periods varying from 10 μs to 1 s. The data are used to extract relative dissociation energies, which agree well with model-free values determined previously by other means, albeit with a slightly larger magnitude of the odd-even effect. Below $n \simeq 24$ the relative dissociation energies extracted from the abundance spectra develop very little over the five orders of magnitude in time covered in the experiments. This behavior has been predicted, but not tested previously. Above $n \simeq 24$ both spectra and dissociation energies develop odd-even effects after a storage time of 10–100 ms. Possible reasons for this behavior are discussed.

PACS. 36.40.Wa Charged clusters – 36.40.Qv Stability and fragmentation of clusters

1 Introduction

Atomic clusters are interesting from both a fundamental point of view and for potential technological applications. An important aspect is the change of cluster properties as their size is varied from a few atoms to the bulk limit [1–3]. This is closely linked to potential technological applications in fields such as catalysis [4], where both the large surface-to-volume ratio as well as the specific electronic or structural properties of certain sizes may be favourable.

In order to investigate the intrinsic properties of the clusters themselves it is helpful to be able to switch off any undesired interactions. For this reason, gas-phase studies play an important role. There are many approaches to free clusters, each with its special appeal. In the present investigation we concentrate on ion trapping which combines two important advantages.

(a) The cluster ensemble can be prepared in detail: The preparation includes a selection of the cluster size of interest, if necessary also of a specific isotopomer. It also includes the temperature, e.g. by letting the clusters cool down or by heating before the actual investigation. In addition, the clusters of interest may not even be produced in the source but be available only after some initial interaction. This can be a reaction with some chemical to form a compound of, e.g., a metal cluster with molecular adsorbants or it may be a charge state different from what is delivered by the source. In many cases, such preparatory steps can be performed at an ion trap.

(b) The clusters are stored as long as necessary. This means one can wait for the reaction (in the literal meaning of the word) after a given interaction and thus probe the time structure of a reaction on a scale up to seconds. In addition, an interaction may be repeated at a later time: for interactions with very small cross-sections the same cluster ensemble may be probed several times. In some respect the transition from molecular beams to particle trapping in atomic and molecular physics is similar to the high-energy physics analogue of the transition from fixed-target experiments with beam dump to storage-ring experiments of colliding beams. Thus if a cluster is not affected by, e.g., a given laser pulse, the interaction may take place a few (or thousands of) pulses later with no need for reproducing the cluster ensemble again and again. On the contrary, the clusters of interest may first be accumulated as one of the preparatory steps, before the actual measurement starts.

The next section gives a short introduction into ion trapping. It is followed by the presentation of experimental results from ClusterTrap, a Penning trap for metal cluster research. In particular, we report on the dissociation of size-selected Au_{30}^+ clusters after multi-photon absorption.

[a] e-mail: alexander.herlert@cern.ch

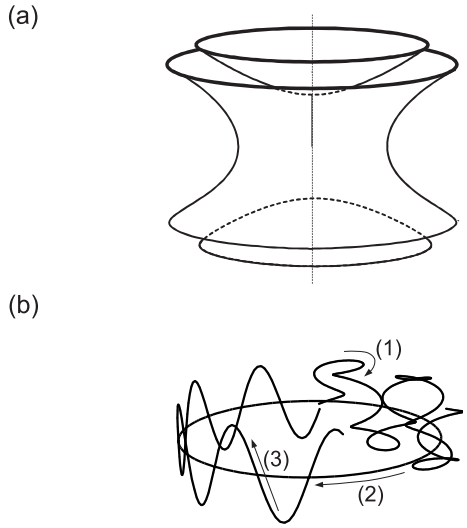

Fig. 1. (a) Ion-trap electrodes as used for Paul and Penning traps. (b) Ion trajectory in a Penning trap, which is composed of three independent motional modes: (1) cyclotron motion, (2) magnetron motion, and (3) trapping motion.

As shown in Section 4, the resulting cluster abundance spectra allow to determine the relative dissociation energies of the fragments Au_n^+, $n < 30$. The experimental data are analyzed by ensemble theory and the resulting relative dissociation energies are compared to values from previous experiments, where each cluster size is addressed by dedicated measurements. This allows a test of the assumptions used to derive the ensemble equations.

2 Ion trapping

Ions may be stored as beams in storage rings based on magnetic bending [5] or electrostatic bending [6] or reflection [7]. These devices certainly have their advantages as, e.g., the possibility to detect low-energy neutral reaction products. However, in the following we will concentrate on devices where the ions are confined at rest in a storage volume of small dimensions. These set-ups can be separated into two major lines, the Paul traps and the Penning traps [8]. As described by the Laplace equation electrostatic forces can not keep a charged particle at one particular spatial position. (Here we assume this position to be free of space charge; in general space-charge confinement, as in an EBIS or EBIT [9], is not compatible with cluster investigations and will be neglected in the following.) Paul traps use only electric fields. However, in order to reach confinement, the polarity is inverted back and forth by use of AC voltages. Typically, voltage signals in the hundreds-of-kHz or few-MHz range are used. Thus, these devices are also called radiofrequency (rf) traps. The effects of the alternating electric field do not cancel entirely if the field is inhomogeneous. In fact, ions are low-field seekers [10]. If the trap electrodes are shaped hyperbolically as shown in Figure 1a, the ions will feel an effective (average) force towards the trap center. What is more, this force is proportional to the distance from the center. Therefore, the ions perform a harmonic so-called macromotion with respect to the trap center. In addition, there is a small-amplitude micromotion which is the ions' immediate response to the rf trapping field, an oscillation at the same frequency with an amplitude proportional to the local electric field. In most cases, the term "Paul trap" refers to such quadrupolar arrangements.

The traditional Penning traps have the same electrode configuration. But in contrast to the Paul traps they rely on static fields, only. In order to reach radial confinement a strong magnetic field is applied. Thus the Lorentz force bends the trajectories of the ions and they perform a circular cyclotron motion. For the axial confinement, parallel to the magnetic field lines, a weak electrostatic field is sufficient. However, this field has also some influence on the radial motion. While it introduces only a small quantitative deviation from the cyclotron frequency in a pure magnetic field, it leads to a qualitative change of the trajectory: In addition to the cyclotron mode it has an independent magnetron mode. The superposition of these modes with the axial trapping mode (Fig. 1b) leads to the complete description of the ion motion [11]. The amplitudes and phases depend on the particular initial conditions of the ions.

Paul traps have a number of advantages: there is no limit with respect to the mass and charge of the particles to be trapped as long as the corresponding trapping parameters are chosen. In particular, heavy particles can be stored; if necessary an additional electric field can be applied to compensate the gravitational force. Furthermore, anions and cations can be stored simultaneously.

In contrast, the axial electrostatic trapping well of the traditional Penning trap provides confinement for only one ion polarity. In addition, there is a limit with respect to the maximum mass (to be more exact the mass-over-charge ratio, m/z) of ions that are to be stored. The limit depends linearly on the magnetic-field strength, which explains the trend to stronger and stronger magnets. And the magnets block the access to the trapping volume of Penning traps, whereas Paul traps can be built in a very open fashion with easy access for ion source and detection and all kinds of photon beams.

On the other hand the magnetic field, as mentioned above, leads to the circular cyclotron motion and its frequency is characteristic of the m/z of the trapped ions. This essentially means that mass spectrometry is a feature which is automatically included. It is extensively made use of in precision mass determination for fundamental studies in nuclear physics, e.g. [12], and elementary particles physics, e.g. [13], as well as for gas-phase ion-molecule reactions in physical chemistry and for sample identification in analytical and biochemistry, e.g. [14]. In addition, the Penning trap allows to simultaneously store particles of very different m/z values, such as heavy (m/z of several thousands) cations together with protons ($m/z = 1$) or anions together with electrons ($m/z \approx 1/2000$). While this feature will not be further discussed in the following, it may be mentioned that it allows

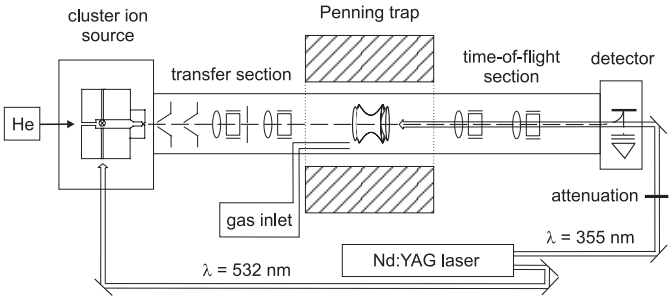

Fig. 2. Schematic overview of the experimental set-up.

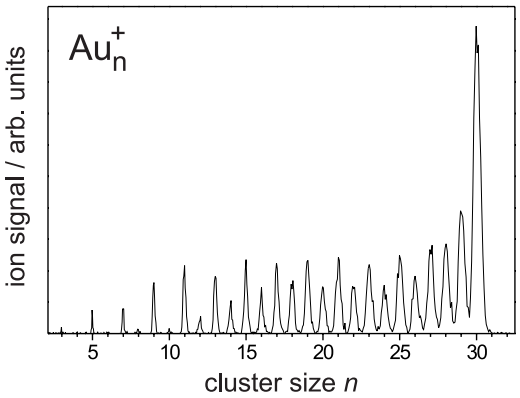

Fig. 3. Time-of-flight spectrum of gold clusters Au_n^+ after photoexcitation of size-selected Au_{30}^+ with a Nd:YAG laser at $\lambda = 355$ nm and 3 mJ pulse energy.

further attachment of electrons and thus the production of polyanionic species [15] and has been used extensively at ClusterTrap [16–18].

3 Photodissociation of size-selected Au_{30}^+ clusters

3.1 Experimental set-up and procedure

The ClusterTrap (Fig. 2) is composed of a cluster source, a transfer section, a Penning trap, a time-of-flight (ToF) drift section and an ion detector. These parts of the vacuum set-up are surrounded by various other devices for the control of the experimental sequences and for data acquisition. The set-up has been reviewed recently [19]. In the following presentation we will only mention the essential features.

The laser-vaporization cluster source [20] has been built at Konstanz [21] and produces singly charged (either cationic or anionic) clusters of elements available as metal wires. The ions are steered by Einzel lenses and deflectors towards the Penning trap, where they are captured in flight [22]. If necessary, several cluster bunches can be accumulated [23]. The ions are centered and cooled by buffer-gas collisions [24] before the actual interaction of interest sets in.

Clusters have been probed by atoms, molecules, electrons and by laser light at various wavelengths [25,26]. After the interaction and a variable delay (or after further interaction events) the ions are axially ejected for ToF mass analysis. Typically, only a few ions are observed (single-ion counting by a Daly-type detector) in a given measurement cycle and 50 mass spectra are added in the present investigation to improve the statistical significance. Between these cycles, i.e. alternating and thus quasi-simultaneously, reference cycles are performed where the interaction in question is switched off. Thus, drifts of the cluster intensity, e.g. due to the source performance, are monitored and accounted for.

For the present experiments a 10-ns Nd:YAG laser was used for both cluster production and excitation. The second-harmonic output (wavelength of 532 nm) was applied for metal vaporization/ionization and the third-harmonic beam of the same laser was used for the photodissociation of the trapped clusters. (The overall laser intensity was controlled by the Q-switch; in addition the intensity of the third-harmonic beam was varied by absorption filters.) Figure 3 shows a typical mass spectrum. While the resolving power is not very high it is sufficient for its purpose, viz. to distinguish the different cluster sizes. The mass abundances were extracted from the spectra by integrating the peaks, without any need for background subtraction.

3.2 Results and discussion

Photoexcitation experiments with multiple dissociation steps have been performed on size-selected Au_{30}^+ clusters. To this end the clusters have been produced, transferred, stored and mass-selected as described above. Note that the laser beam for dissociation has been focused and that thus the laser fluence was not constant across the trap volume.

In Figure 4 the cluster-size distribution is given for a constant delay of 1 s between the irradiation and the mass analysis at various laser-pulse energies. Already at a pulse energy of 3 mJ multiple dissociation is observed. A characteristic feature of the product distributions is the well-known odd-even alternation in the abundance [27,28]. Higher abundance is usually associated with higher stability in accordance with the expected higher stability of the odd-size Au_n^+ clusters, although the connection between high abundance and high stability is not completely trivial, cf. equation (3) below. Since gold is a monovalent element, odd numbered cluster sizes contain an even number of valence electrons and vice versa.

In order to study the general trend, the odd-even effect can be smoothed by averaging intensities as $I_n/2 + I_{n+1}/4 + I_{n-1}/4$. The corresponding lines are plotted in Figure 4 (bottom). When the laser-pulse energy is increased to 6 and 10 mJ (see again Fig. 4), the abundance distribution shifts to smaller clusters as the clusters absorb more photons; the increased excitation energy leads to the loss of more atoms. As a typical dissociation energy for the evaporation of one atom is similar to the photon

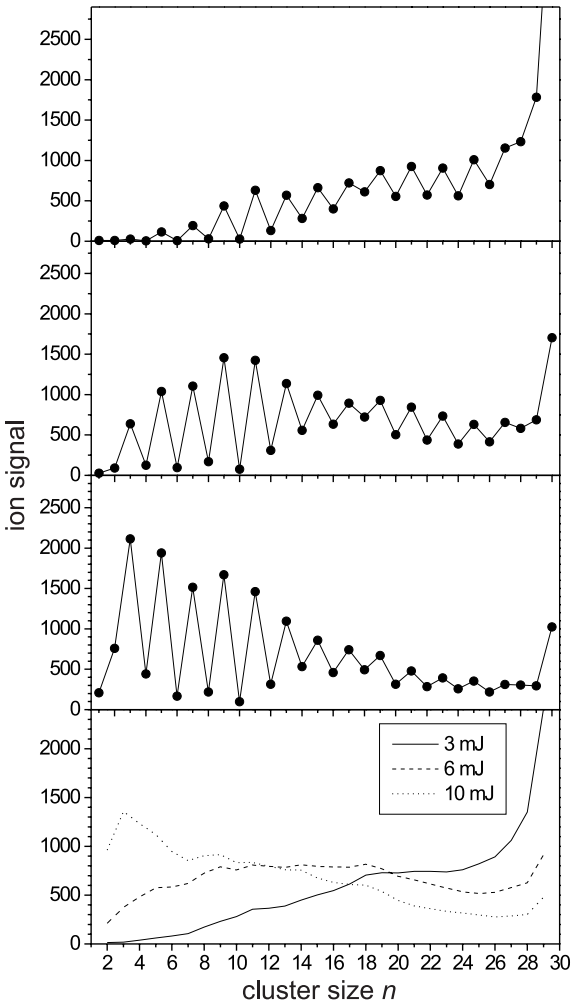

Fig. 4. Top to bottom: number of ions as a function of cluster size n for laser pulse energies of 3 mJ, 6 mJ, 10 mJ, and averaged ion numbers (see text).

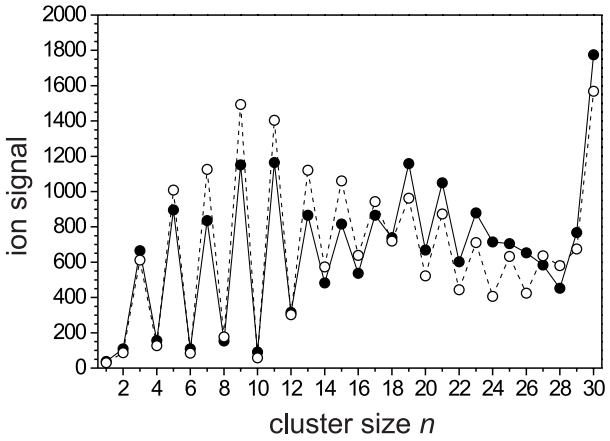

Fig. 5. Number of ions as a function of cluster size n for delay times between photoexcitation and ToF mass analysis of 10 μs (filled circles, solid line) and 1 s (open circles, dashed line).

energy, the decay from Au_{30}^+ to, e.g., Au_{20}^+ involves the absorption of about 10 photons.

A delay of one second is presently at the border of what can be monitored time-resolved at ClusterTrap. The limiting factor is determined by the vacuum conditions and the corresponding average time between collisions with residual gas molecules. The other end of the time-scale is given by the ejection of the clusters from the trap and acceleration for the ToF analysis. It is on the order of ten microseconds. In Figure 5 the abundance spectra for different delay times are compared for a laser-pulse energy of 6 mJ. The decay shows some temporal behavior: the center of the fragments shifts only little, but the abundance structure develops more pronounced features as time elapses, in particular for the larger masses: Initially there is no odd-even alternation at all close to the precursor size; this structure is fully developed at later times.

The reason for this behavior is not fully understood but several possibilities present themselves. Note that the change of a particular cluster-size signal is not only related to the decay of this cluster but also to the feeding from decays of higher-size clusters. Furthermore, this decay may not only take place in the form of single-atom evaporation, as for the larger gold clusters, but may also come in competing decay channels: in the case of the smaller gold clusters dimer emission can compete or even be the dominant decay channel [29].

The odd-even effect in the mass spectra may grow with time because the clusters with even electron numbers stop decaying before those with an odd electron. This happens if they have a stronger radiative cooling [30–32] than the odd-electron clusters, causing an earlier quenching of the decay, whereas the odd clusters continue to decay and enrich the even clusters. Alternatively, it may happen because the odd-even effect is intrinsically temperature dependent and increases with time because the internal energy (temperature) decreases with time. Finally it may be due to a time dependence of the monomer-dimer competition. This is expected to happen because the two channels have different activation energies, and the clusters cool with time, causing a time variation of the Boltzmann factors associated with the two processes. The dedicated measurements of the time dependence of the decay branching ratios in [29] for Au_n^+, $n < 28$, did not show any time dependence, but these measurements refer to clusters with well defined excitation energy, contrary to the present situation.

4 Further data analysis

The shapes of the mass spectra depend on a number of parameters, like laser-pulse energy, photo-absorption cross-section, laser-pulse profile, dissociation energies, and trap-extraction time. It is likely that the spectra can be reproduced with suitable parameters, but we also expect that these parameters are not unique and that several sets of values can give good agreement. We will therefore not attempt to take all these factors into account, but instead focus on specific features of the spectra. In particular, this will lead to a determination of the relative

dissociation energies as a function of cluster size. These relative dissociation energies will be compared with independent previous measurements [33], primarily as a test of the assumptions used to derive the relation between ensemble abundance and dissociation energy, viz. no radiative cooling and an equipartition heat capacity. A similar comparison has previously been made on large sodium clusters with ensembles of freely evaporating clusters and measurements of thermal activation energies in heat bath experiments [34,35].

Since the clusters are isolated in a "wall-less vacuum container" the decay will not be determined by the temperature of any heat bath, but rather by the excitation energy which, disregarding radiative cooling, is conserved between decays. It can be shown, under certain conditions, that the observed decay rate for a specific cluster size in these ensembles follows a simple powerlaw over a broad time interval [36]. The conditions are that the energy-specific rate constants depend strongly on energy, that only one decay channel is present, and that the distribution of excitation energies is sufficiently flat. The present time intervals are very long, but the proper modifications to the powerlaw decay are easily made. The correction involves the value of the Gspann parameter [37], $G = \ln(\omega t)$, where ω is the frequency factor in the unimolecular decay rate constant, and t is the observation time. In [34] the decay rates are calculated to be

$$R(t) = \frac{C_v}{k_B(\ln(\omega t))^2}\frac{1}{t}, \tag{1}$$

where C_v is the heat capacity of the cluster considered.

Summing this decay rate over all sizes and integrating over time gives the total change in average cluster size $\overline{n}$ from t_1 to t_2. The average number of lost atoms relative to the parent is then given by

$$\Delta\overline{n} = \Delta\overline{n}(t_1) + \frac{C_v(\overline{n}(t_1))}{k_B}\left(\frac{1}{\ln(\omega t_1)} - \frac{1}{\ln(\omega t_2)}\right), \tag{2}$$

where $C_v(\overline{n})$ is the heat capacity of the average size. Heat capacities are assumed to be $(3n-6)k_B$, and hence $C_v(\overline{n}) = k_B(3\overline{n}(t_1) - 6)$, a number which changes only little from 10 μs to 1 s because $\overline{n}$ only changes little. The experimental values for $\Delta\overline{n}$ are shown in Figure 6 (filled circles), together with the expected theoretical curve (dashed line) calculated with $\omega = 10^{16}\,\mathrm{s}^{-1}$. The $\Delta\overline{n}(10\,\mu\mathrm{s})$ summarizes the unknown factors in the excitation, and is fitted to the value 12.3. The data points and the curve are in reasonable agreement.

The decay rates used above are based on the existence of a highest excitation energy for a given cluster size in the ensemble at a given time after excitation. With the same assumptions one can also derive a relation between abundances I_n and dissociation energies D_n and D_{n+1} [34,38]:

$$I_n \propto \frac{D_n + D_{n+1}}{2} + \frac{C_v(n)}{k_B}\frac{D_n}{G} - \frac{C_v(n+1)}{k_B}\frac{D_{n+1}}{G}. \tag{3}$$

We have furthermore assumed that the last evaporation is thermal. The constant of proportionality is a smooth

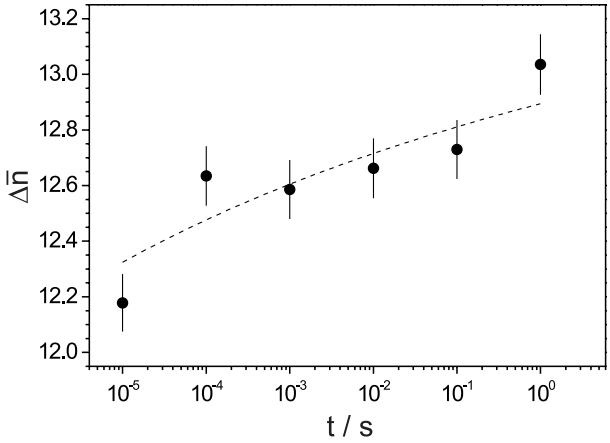

Fig. 6. Average number of lost atoms $\Delta\overline{n}$ with respect to the parent cluster as a function of the delay time t between excitation and ToF mass analysis.

function of size, and includes the secular variations of the abundances as well as the size-dependence of the dissociation energies. Typically, the latter can be estimated with the liquid-drop parameters, but at present this is not needed. The analysis is akin to the shell correction method borrowed from nuclear physics and used previously in the analysis of both theoretical and experimental data on electronic shell structure [3].

The equation can be inverted to find the dissociation energies relative to the smooth part of the D vs. n curve, i.e. essentially the liquid drop values. To this end, the secular variations of the abundances must be divided out. This is achieved by dividing with the function, derived from the measured data themselves,

$$\widetilde{I}_n = \frac{\sum_m I_m \exp(-(n-m)^2/5)}{\sum_m \exp(-(n-m)^2/5)}. \tag{4}$$

The width of the Gaussian used to calculate this average is not critical. Replacing the value 5 with larger values mainly induces a low frequency drift with no change of the relative size-to-size variations.

The result of the inversion is shown in Figure 7 for cluster sizes $n > 14$. Below this range the dimer channel is finite and equation (3) does not apply. The recurrence is initiated by assuming a scaled value of $D_{30} = 1$, and as expected the values vary around unity. The analysis for different times differ only in the value of G, which varies from 25.3 ($t = 10\,\mu$s) to 36.8 ($t = 1$ s).

Values determined in a model-free way by comparison of sequential and single-step decays [33,39] are plotted with open circles. For comparison these values have been divided with a second order polynomial, and a constant added for display purposes. The error bars include an estimated systematic uncertainty, and are probably exaggerated in this representation. The general agreement is fairly good, although the inverted abundance spectra have odd-even effects which are larger than those of the model-free numbers. (The small drift with size cannot be expected to be reproduced exactly with the methods applied.) Note that the values agree nicely for $n = 15$ to

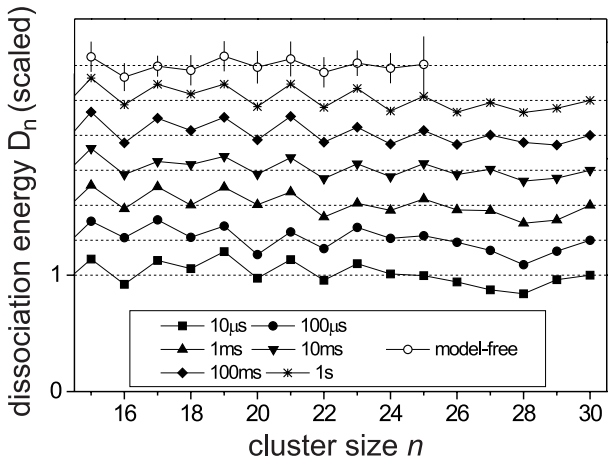

Fig. 7. Scaled dissociation energies of gold clusters Au_n^+, $15 \leq n \leq 30$, for different delay times between photoexcitation and ToF mass analysis. The dashed lines indicate a value of 1. The data for different times are displaced by 0.3 for display purposes. For comparison, the model-free dissociation energies [33] are plotted with open circles.

$n = 26$, while there are large disagreements for the bigger clusters. The bigger the cluster size, the longer one has to wait before the differences in intensities and dissociation energies show up. With the present data it is not possible to say whether this is an intrinsic property of these cluster sizes or a consequence of the proximity in size of the precursor.

The data have been analyzed with the assumption that no radiation occurs. While this kind of cooling may have to be included, the corresponding radiative quenching will occur at approximately the same time scales for all clusters. Although this seems to require a finetuning of the radiative cooling, it is in fact not needed: consider a situation where the cluster size $n+1$ effectively stops decaying at time t_{n+1}, while size n continues to decay until time $t_n > t_{n+1}$. During this time interval, cluster size n is depleted by the amount

$$\delta I_n \propto \int_{t_{n+1}}^{t_n} \frac{C_v(n)}{k_B(\ln(\omega t))^2 t} dt \tag{5}$$

$$= \frac{C_v(n)}{k_B}\left(\frac{1}{\ln(\omega t_n)} - \frac{1}{\ln(\omega t_{n+1})}\right) \tag{6}$$

$$= \frac{C_v(n)}{k_B}\frac{\ln(t_{n+1}/t_n)}{\ln(\omega t_n)\ln(\omega t_{n+1})}. \tag{7}$$

The odd-even effects in the abundance spectra are on the order of unity above $n \approx 12$. Hence we must require that $\delta I_n \ll 1$ in between the two times. The heat capacity $(3n-6)k_B$ and the two logarithms (≈ 30) combine to give the approximate inequality

$$\ln(t_n/t_{n+1}) \ll \frac{300}{n}. \tag{8}$$

This inequality is surprisingly weak, and we expect it to be fulfilled for the moderate cluster sizes of the present study.

5 Summary, conclusion and outlook

As described in the Introduction, ion trapping offers several advantages for the study of atomic clusters. In the present case study on Au_{30}^+ it has been described how clusters can be size-selected and further prepared in a Penning trap, excited by laser light and mass analyzed after a variable delay. Thus their multisequential decay can be monitored by time-resolved mass spectrometry. The abundance evaluation leads to the determination of relative dissociation energies of the clusters in the decay chain. Absolute dissociation energies are known for the clusters studied, and the studies presented here serve as a test of the assumed thermal properties of the clusters. The two different determinations are in reasonable agreement below $n \approx 24$, but the discrepancies, and the timedependence of the fitted dissociation energy at higher masses suggest the presence of unaccounted effects.

Note that, while the present laser-pulse energy is not small, it is spread within a rather large period of about ten nanoseconds. An increase of the irradiation by use of picosecond or femtosecond laser pulses will provide events which are much more violent than the present ones. For such new experiments ion storage will still provide the ideal conditions of cluster accumulation and preparation, in particular with respect to cluster-size selection. However, many product ions may be relatively energetic, i.e. they will have a high kinetic energy and thus will not stay stored inside the trap for further analysis. Therefore the trap will no longer be able to serve as a 4π detector. On the other hand, faster decays may be accessible in a time-resolved manner, if the products can fly directly towards appropriate detectors. To allow such a detection a more open structure than at the present set-up will be needed. As explained above (Sect. 2 on ion trapping) Penning traps in general do not allow open structures. Thus, we plan to develop open-structured Paul traps for the direct monitoring of highly energetic products of cluster decays by intense laser irradiation.

This work has been partly supported by the EU under contract no. IHP-CT-2000-00026 and by the Swedish Research council VR.

References

1. J. Jortner, Z. Phys. D **24**, 247 (1992)
2. W.A. de Heer, Rev. Mod. Phys. **65**, 611 (1993)
3. M. Brack, Rev. Mod. Phys. **65**, 677 (1993)
4. M. Haruta, Catalysis Today **36**, 153 (1997)
5. K. Abrahamsson, G. Andler, L. Bagge, E. Beebe, P. Carlé, H. Danared, S. Egnell, K. Ehrnstén, M. Engström, C.J. Herrlander, J. Hilke, J. Jeansson, A. Källberg, S. Leontein, L. Liljeby, A. Nilsson, A. Paal, K.-G. Rensfelt, U. Rosengård, A. Simonsson, A. Soltan, J. Starker, M. af Ugglas, Nucl. Instr. Meth. B **79**, 269 (1993)
6. S.P. Møller, Nucl. Instr. Meth. A **394**, 281 (1994)
7. A. Naaman, K.G. Bhushan, H.B. Pedersen, N. Altstein, O. Heber, M.L. Rappaport, R. Moalem, D. Zajfman, J. Chem. Phys. **113**, 4662 (2000)

8. F.G. Major, V.N. Gheorghe, G. Werth, *Charged Particle Traps, Physics and Techniques of Charged Particle Field Confinement*, Springer Series on Atomic, Optical, and Plasma Physics, Vol. 37, Springer, Berlin, 2005)
9. M.A. Levine, R.E. Marrs, J.R. Henderson, D.A. Knapp, M.B. Schneider, Phys. Scripta T **22**, 157 (1988)
10. D. Gerlich, in *Advances in Chemical Physics* (John Wiley & Sons, New York, 1992), Vol. LXXXII, pp. 1-176
11. L.S. Brown, G. Gabrielse, Rev. Mod. Phys. **58**, 233 (1986)
12. K. Blaum, G. Audi, D. Beck, G. Bollen, P. Delahaye, S. George, C. Guénaut, F. Herfurth, A. Herlert, A. Kellerbauer, H.-J. Kluge, D. Lunney, M. Mukherjee, S. Schwarz, L. Schweikhard, C. Yazidjian, Nucl. Phys. A **752**, 317c (2005)
13. G. Gabrielse, N.S. Bowden, P. Oxley, A. Speck, C.H. Storry, N. Tan, M. Wessels, D. Grzonka, W. Oelert, G. Schepers, T. Sefzick, J. Walz, H. Pittner, T.W. Hänsch, E.A. Hessels, Phys. Rev. Lett. **89**, 213401 (2002)
14. A.G. Marshall, C.L. Hendrickson, G.S. Jackson, Mass Spectrom. Rev. **17**, 1 (1998)
15. A. Herlert, S. Krückeberg, L. Schweikhard, M. Vogel, C. Walther, Phys. Scripta **T80**, 200 (1999)
16. L. Schweikhard, A. Herlert, S. Krückeberg, M. Vogel, C. Walther, Philos. Mag. B **79**, 1343 (1999)
17. C. Yannouleas, U. Landman, A. Herlert, L. Schweikhard, Phys. Rev. Lett. **86**, 2996 (2001)
18. A. Herlert, L. Schweikhard, Int. J. Mass Spectrom. **229**, 19 (2003)
19. L. Schweikhard, K. Hansen, A. Herlert, G. Marx, M. Vogel, Eur. Phys. J. D **24**, 137 (2003)
20. T.G. Dietz, M.A. Duncan, D.E. Powers, R.E. Smalley, J. Chem. Phys. **74**, 6511 (1981)
21. H. Weidele, U. Frenzel, T. Leisner, D. Kreisle, Z. Phys. D **20**, 411 (1991)
22. H. Schnatz, G. Bollen, P. Dabkievicz, P. Egelhof, F. Kern, H. Kalinowsky, L. Schweikhard, H. Stolzenberg, H.-J. Kluge, The ISOLDE Collaboration, Nucl. Instr. Meth. A **251**, 17 (1986)
23. H.-U. Hasse, St. Becker, G. Dietrich, N. Klisch, H.-J. Kluge, M. Lindinger, K. Lützenkirchen, L. Schweikhard, J. Ziegler, Int. J. Mass Spectrom. Ion Proc. **132**, 181 (1994)
24. G. Savard, St. Becker, G. Bollen, H.-J. Kluge, R.B. Moore, Th. Otto, L. Schweikhard, H. Stolzenberg, U. Wiess, Phys. Lett. A **158**, 247 (1991)
25. U. Hild, G. Dietrich, S. Krückeberg, M. Lindinger, K. Lützenkirchen, L. Schweikhard, C. Walther, J. Ziegler, J. Chem. Phys. **57**, 2786 (1998)
26. G. Dietrich, S. Krückeberg, K. Lützenkirchen, L. Schweikhard, C. Walther, J. Chem. Phys. **112**, 752 (2000)
27. C. Jackschath, I. Rabin, W. Schulze, Ber. Bunsen Ges. Phys. Chem. Chem. Phys. **96**, 1200 (1992)
28. M. Manninen, J. Mansikka-aho, H. Nishioka, Y. Takahashi, Z. Phys. D **31**, 259 (1994)
29. M. Vogel, K. Hansen, A. Herlert, L. Schweikhard, Eur. Phys. J. D **16**, 73 (2001)
30. K. Hansen K, E.E.B. Campbell, Phys. Rev. E **58**, 5477 (1998)
31. C. Walther, G. Dietrich, W. Dostal, K. Hansen, S. Krückeberg, K. Lützenkirchen, L. Schweikhard, Phys. Rev. Lett. **83**, 3816 (1999)
32. J.U. Andersen, C. Gottrup, K. Hansen, P. Hvelplund, M.O. Larsson, Eur. Phys. J. D **17**, 189 (2001)
33. M. Vogel, K. Hansen, A. Herlert, L. Schweikhard, Phys. Rev. Lett. **87**, 013401 (2001)
34. K. Hansen, U. Näher, Phys. Rev. A **60**, 1240 (1999)
35. J. Borggreen, K. Hansen, F. Chandezon, T. Døssing, M. Elhajal, O. Echt, Phys. Rev. A **62**, 013202 (2000)
36. J.U. Andersen, E. Bonderup, K. Hansen, P. Hvelplund, B. Liu, U.V. Pedersen, S. Tomita, Eur. Phys. J. D **24**, 191 (2003)
37. K. Hansen, E.E.B. Campbell, Int. J. Mass Spectrom. **233**, 215 (2004)
38. S. Prasalovich, K. Hansen, M. Kjellberg, V. Popok, E.E.B. Campbell, J. Chem. Phys. **123**, 084317 (2005)
39. M. Vogel, K. Hansen, A. Herlert, L. Schweikhard, J. Phys. B: At. Mol. Opt. Phys. **36**, 1073 (2003)